Solid State Communications 249 (2017) 19–23

Contents lists available at ScienceDirect

Solid State Communications

journal homepage: www.elsevier.com/locate/ssc

Communication

Correlation between electrical, magnetocaloric properties and critical behavior in $(La_{0.75}Nd_{0.25})_{2/3}(Ca_{0.8}Sr_{0.2})_{1/3}MnO_3$

J. Khelifi[a,b,c,*], E. Dhahri[a], E.K. Hlil[d]

[a] Laboratoire de Physique Appliquée, Faculté des Sciences de Sfax, Université de Sfax, B. P. 1171, 3000 Sfax, Tunisia
[b] Faculté des Sciences de Gafsa, Campus Universitaire Sidi Ahmed Zarroug, 2112 Gafsa, Tunisia
[c] Unité de recherche Valorisation et optimisation de l'exploitation des ressources, Faculté des Sciences et Techniques de Sidi Bouzid, Campus Universitaire Cité Agricole, 9100 Sidi Bouzid, Tunisia
[d] Institut Néel, CNRS et Université Joseph Fourier, BP 166, 38042 Grenoble, France

ARTICLE INFO

Keywords:
Manganites
Magnetocaloric effect
Critical behavior
Resistivity

ABSTRACT

An investigation of the critical behavior and magnetic entropy from resistivity of $(La_{0.75}Nd_{0.25})_{2/3}(Ca_{0.8}Sr_{0.2})_{1/3}MnO_3$ is presented. The magnetocaloric properties of the polycrystalline manganite $(La_{0.75}Nd_{0.25})_{2/3}(Ca_{0.8}Sr_{0.2})_{1/3}MnO_3$ based on resistivity measurements were investigated. Using, the equation $\Delta S = -\alpha \int_0^H \frac{\partial Ln(\rho)}{\partial T})_H dH$ relates magnetic order to the transport behavior of the compound, we measure the magnetic entropy change ΔS_M from the resistivity which is similar to that calculated from the magnetic measurement. Moreover, we have found an excellent estimation of critical behavior from resistivity and magnetic analysis.

1. Introduction

Manganites $Re_{1-x}A_xMnO_3$ (Re=La, Pr, Nd... and A=Ca, Sr, Ba...) are the focus of contemporary research activity in order to understand their complex phase diagram, metal insulator transition, most importantly colossal magnetoresistance (CMR) and magnetocaloric properties (MCE) [1–3]. The CMR and MCE are usually observed in the vicinity of the magnetic phase transition temperature, and, obviously, there is interesting correlations between the transport properties such as resistivity and the change of the magnetic entropy. This relation was described by Xiong et al. [4] who proposed a new method for evaluating the change of the magnetic entropy from data on the temperature and field dependences of the electrical resistivity of manganites. One of the fundamental characteristics of perovskite materials concerns the strong correlation between electrical and magnetocaloric properties. This method has been recently studied and presented in several works in the literature [5–7]. They suggested that the relation between ΔS_M and resistivity ρ in manganites can be expressed as $\Delta S = -\alpha \int_0^H \frac{\partial Ln(\rho)}{\partial T})_H dH$, where the parameter α determines the magnetic properties of the sample.

The electrical, magnetic properties and the magnetocaloric effect in manganites are studied quite a lot [8–11]. We noted that most of the previous studies concentrated on the relation between magnetization and resistivity. Indeed, magnetic entropy is also a parameter often used to characterize magnetic order. In fact, the relation between magnetic entropy and transport behavior has been raised in few previous studies [12,13]. Considering the fact that magnetic disorder has a strong effect on the resistive behavior of the manganites, we expect a definite relation between these two quantities.

In this paper, the magnetic entropy change (ΔS_M) based on electrical results has been investigated. On the other hand, we report an estimation of the critical exponents of second order phase transition from the resistivity measurements under applied magnetic field using the Fisher–Langer relation and the Suezaki - Mori method.

2. Experimental details

A polycrystalline sample of nominal composition $(La_{0.75}Nd_{0.25})_{2/3}(Ca_{0.8}Sr_{0.2})_{1/3}MnO_3$ was prepared according to the solid state reaction method at high temperature. The detailed preparation procedure and basic physical properties are reported in our previous work [14]. The resistivity measurements with magnetic field are carried out using four-probe method in the temperature range from 2 to 400 K on a quantum design Physical Property Measurement System (PPMS Model). Magnetic measurements were realized with the *BS2* magnetometer developed at Néel Institute.

* Corresponding author at: Laboratoire de Physique Appliquée, Faculté des Sciences de Sfax, Université de Sfax, B. P. 1171, 3000 Sfax, Tunisia.
E-mail address: klifijaber@yahoo.fr (J. Khelifi).

http://dx.doi.org/10.1016/j.ssc.2016.10.010
Received 13 May 2016; Received in revised form 23 September 2016; Accepted 17 October 2016
Available online 18 October 2016
0038-1098/

Table 1
Crystallographic data deduced from the Rietveld refinement of X-ray diffraction data for $(La_{0.75}Nd_{0.25})_{2/3}(Ca_{0.8}Sr_{0.2})_{1/3}MnO_3$.

Sample	$(La_{0.75}Nd_{0.25})_{2/3}$ $(Ca_{0.8}Sr_{0.2})_{1/3}MnO_3$
$\sigma^2 \times 10^{-3}$ (Å^2)	1.335
a (Å)	5.4607(0)
b (Å)	7.7169(40)
c (Å)	5.4753(6)
(La, Ca, Nd, Sr) x	−0,0207
Z	0,0034
(Mn) x	0.00
Y	0.00
Z	0.50
O(1) x	0,5078
Z	0,9288
O(2) x	0,7743
Y	−0,0304
Z	0,7863
v (Å^3)	230.73(1)
< *Mn-O* > (Å)	1.9668(9)
< *Mn-O-Mn* >	161.105(5)
R_P	17.2
R_{wp}	22.2
χ^2	1.84
D(x10^{-3}%)	0,0169
D_{MEB}(µm)	2216
D_{SC} (µm)	0, 733
X-ray density d_X (g/cm^3)	2172

3. Results and discussion

3.1. Structure and morphology

The phase identification, based on X-ray diffraction results, is showed in ref.[14]. The Rietveld refinements of the XRD data performed using FULLPROF program [15] revealed that this compound crystallized in the orthorhombic structure with the *Pnma* space group. The refined structural parameters obtained are included in Table 1.

It is worth mentioning that for $(La_{0.75}Nd_{0.25})_{2/3}(Ca_{0.8}Sr_{0.2})_{1/3}MnO_3$ sample ($b/\sqrt{2} \leq a \leq c$). This is characteristic of the so-called O'' type orthorhombic structure and it is originated from the strong cooperative Jahn–Teller effect, inducing an orbital ordering and distorting the MnO_6 octahedra [16]. The orthorhombic deformation is defined as:

$$D = \frac{1}{3}\sum_i \frac{a_i - \langle a \rangle}{\langle a \rangle} x100 \quad (1)$$

Where $\langle a \rangle = (a.\ b.\ c/\sqrt{2})^{1/3}$ and a_i is the lattice parameter.

The larger deformation in $(La_{0.75}Nd_{0.25})_{2/3}(Ca_{0.8}Sr_{0.2})_{1/3}MnO_3$ might be attributed to the effect of disorder present in the sample.

We have also estimated the average grain size D_{sc} from XRD patterns using the Scherrer formula [17]:

$$D_{SC} = \frac{0.9 \times \lambda}{\beta \times \cos\theta} \quad (2)$$

Where λ is the used wavelength, θ is the Bragg angle for the most intense peak and β is the half-height width of this peak. Moreover, we calculated the X-ray density, $d_x = M/N.a^3$ [18], where M is the molecular weight, N is the Avogadro's number and a is the lattice constant.

In order to evaluate the existence of all the elements in $(La_{0.75}Nd_{0.25})_{2/3}(Ca_{0.8}Sr_{0.2})_{1/3}MnO_3$ compound, energy dispersive X-ray analysis (EDAX) were performed parallel to the Scanning Electron Microscope (SEM) observations. Fig. 1 shows a typical (EDAX) spectrum for the $(La_{0.75}Nd_{0.25})_{2/3}(Ca_{0.8}Sr_{0.2})_{1/3}MnO_3$ sample. The spectrum contains characteristic peaks of La, Nd, Ca, Sr and Mn which confirm that there is no loss of any integrated element after sintering. So they are all non-volatile at 1400 K. Furthermore, to examine the morphology of our specimen, we used the SEM as reported in the inset of Fig. 1. The nature and distribution of microstructures suggest the formation of a single-phase compound. The micrograph reveals the existence of a polycrystalline nature of the sample. It is found that the grains are homogeneously distributed throughout the surface of the material. The average size of the particle of the samples is calculated using the Scanning Electron Microscope (SEM) images by finding the minimum and maximum dimension of the large number of particles(A manual statistical count of grain size has been performed). One can notice that the grains are irregularly spherical like and the mean size is varying between 1 and more than 2 µm. We summarized in Table 1 the X-ray density (d_x), the grain size D_{sc} and D_{MEB} values. The significant difference between D_{SEM} and D_{SC}, which indicates that each particle observed by SEM basically consist of several crystalline grains [18].

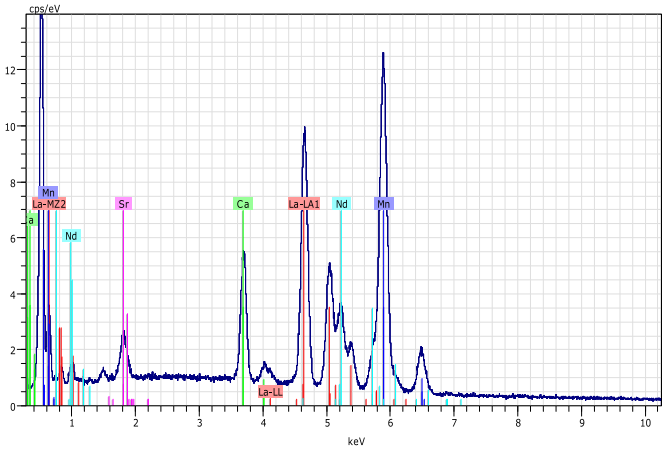

Fig. 1. Chemical analysis EDAX for $(La_{0.75}Nd_{0.25})_{2/3}(Ca_{0.8}Sr_{0.2})_{1/3}MnO_3$ sample. Inset: SEM photos obtained for $(La_{0.75}Nd_{0.25})_{2/3}(Ca_{0.8}Sr_{0.2})_{1/3}MnO_3$ compound.

3.2. Magnetic entropy from resistivity

Many researchers have shown a strong correlation between electrical and magnetic properties [19,20]. In manganite materials, the CMR and MCE effects are usually observed near the magnetic phase transition temperature. It is obvious that there is some relation between the change in magnetic entropy and resistivity. In this context, Xiong et al. [4] proposed a relationship between ΔS_M and ρ given by:

$$\Delta S = -\alpha \int_0^H \left(\frac{\partial Ln(\rho)}{\partial T}\right)_H dH;\ \cdot = a = 21;\ 74\ emu/g \quad (3)$$

Where the parameter α determines the magnetic properties of the sample. Different relation between M and ρ have been used to estimate α directly where $\rho = \rho_0 exp(-M/\alpha)$[4]. O'Donnell et al. [19] noted that the equation should be expressed as $\rho = \rho_0 exp(-M^2/\alpha)$, whereas Chen et al. [20] proposed the equation: $\rho = \rho_0 exp(-M^2/\alpha T)$ for small and intermediate magnetization near and above the Curie temperature.

According to the ρ (H, T) curves plotted in Fig. 2, the magnetic entropy change (ΔS_M) have been estimated using Eq. (3), for an applied magnetic field of 3 T. For this purpose the variation ρ versus M (a), M^2(b) and M^2/T (c) was presented in Fig. 3. These studies have shown that the resistivity strongly depends on M^2/T. For $(La_{0.75}Nd_{0.25})_{2/3}(Ca_{0.8}Sr_{0.2})_{1/3}MnO_3$ sample, we found that α determined from the fitting of ρ versus M^2/T curve around the transition temperature T_C with the equation: $\rho = \rho_0 exp(-M^2/\alpha T)$(Fig. 3) has the order of 175.86 $(emu)^2/g^2K$. Similar results have been obtained by M. Patra et al. [21] in a different way, and the value proposed is α=240 emu/g for $La_{0.7}Ba_{0.3}MnO_3$ compound.

The entropy change determined by the resistivity measurement and the Maxwell relation, described in our previous research work [22], are shown in Fig. 4. The calculated ΔS_M values from the temperature

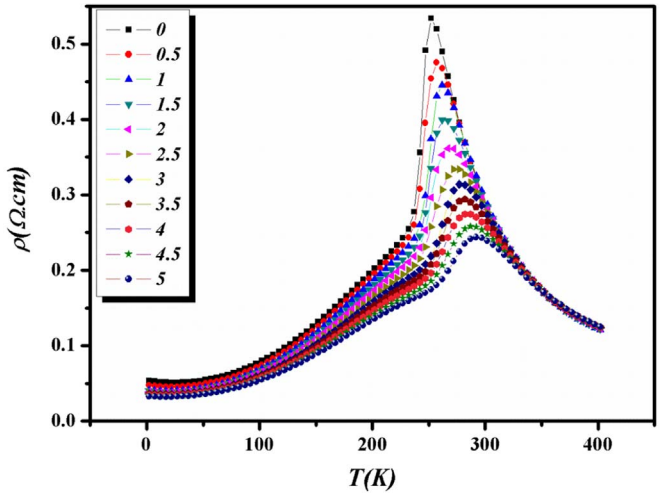

Fig. 2. Variation of resistivity as function of temperature versus magnetic field.

dependence of the resistivity were found to present a similar maximum of the magnetic entropy change deduced from the experimental M(H, T) curves, around the Curie temperature T_C. The small difference between the two curves can be explained by the strong electron–phonon interactions as well as by the effect of the disorder on the electrical properties [23,24].

This result implies that the resistivity measurements are in agreement with the magnetic data mainly in the intermediate temperature range, i.e., during the establishment of perfect ferromagnetic order.

3.3. Calculation of critical exponents from resistivity

The systems which show second order metal-insulator phase transition obey one of the common universality classes such as mean field, three dimensional Heisenberg, three dimensional Ising [25] and tricritical mean field [26]. These models have unique values for set of critical exponents. Hence, determining the values of critical exponents close to second order metal-insulator transition, and assigning of one of these models to second order systems have been extremely useful for better understanding the nature of phase transition.

3.3.1. Specific heat critical exponent (α)

According to the Fisher–Langer theory [27], specific heat at constant pressure (Cp) and at the phase transition temperature is proportional to the temperature derivative of the resistivity at $T=T_{MI}$. The thermal derivative of the resistivity is given by Fisher–Langer as:

$$Cp \propto \left(\frac{d\rho}{dT}\right) = \left(\frac{d\rho}{d\eta}\right) = \eta^{-\alpha} \tag{4}$$

Where α is the specific heat critical exponent, C_p is the specific heat and $\eta = [T - T_{MI}/T_{MI}]$ is the reduced temperature.

$$C(T) = \left[\frac{1}{\rho(T_{MI})}\frac{d\rho}{dT}\right] = \frac{A^+}{\alpha}[(-\eta)^{-\alpha} - 1] + B^+ \; for \; T < T_{MI} \tag{5}$$

$$C'(T) = \left[\frac{1}{\rho(T_{MI})}\frac{d\rho}{dT}\right] = \frac{A^-}{\alpha'}[(-\eta)^{-\alpha'} - 1] + B^- \; for \; T > T_{MI} \tag{6}$$

Where A and B are constants, α and α′ are specific heat critical exponents below and above T_{MI}.

The temperature derivative of resistivity normalized with respect to its value at T_{MI} $[(1/\rho(T_C))(d\rho/dT)]$ against η is shown in Fig. 5 and the Eqs. (5) and (6) are fitted below and above T_{MI} in the same figures.

The solid lines passing through the data are the best fit in the two regions. The values of specific heat critical exponents below and above T_{MI}, (α and α′) are obtained from the fitting analysis, and the values

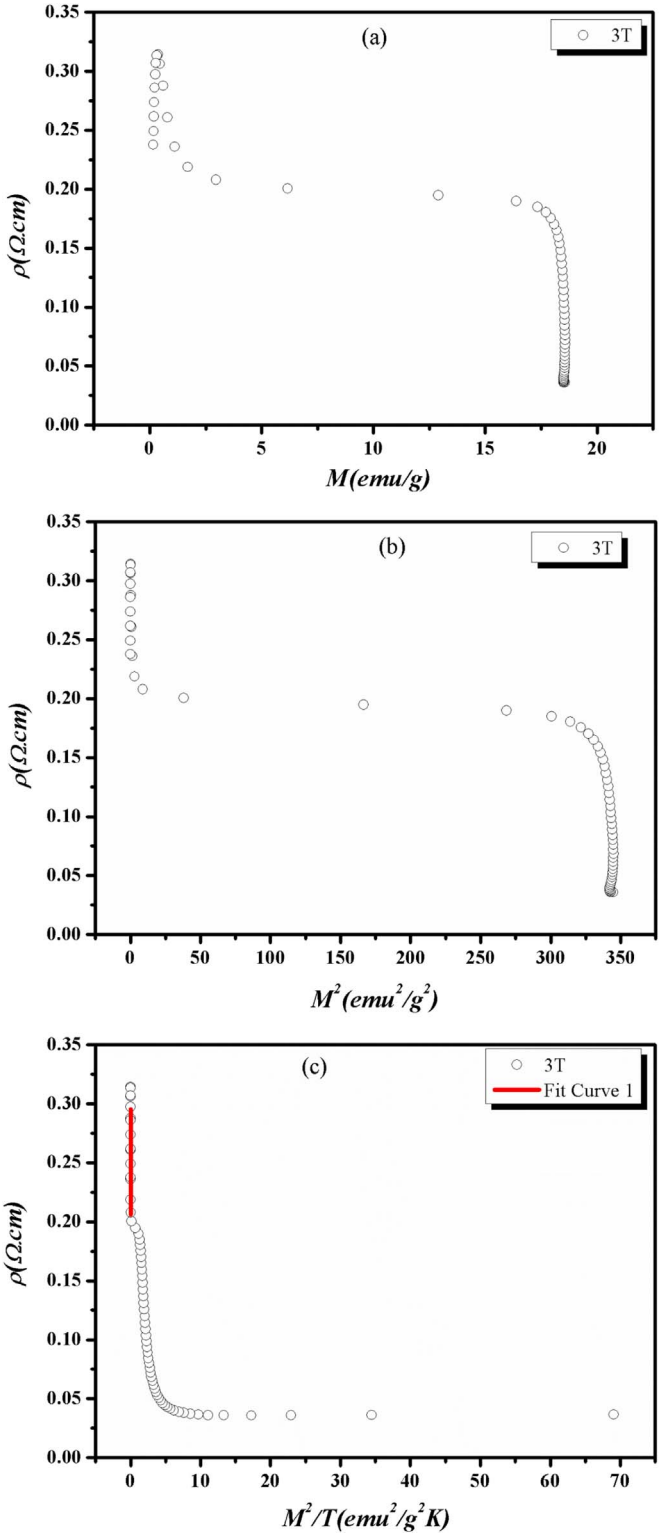

Fig. 3. ρ versus M (a), M^2 (b) and M^2/T (c) for $(La_{0.75}Nd_{0.25})_{2/3}(Ca_{0.8}Sr_{0.2})_{1/3}MnO_3$ sample, under the field of 3 T. Solid line is a fit to the formula $\rho = \rho_0 exp(-M^2/\alpha T)$.

are given in Table 2.

It is clear from Table 2 that the specific heat critical exponents for $(La_{0.75}Nd_{0.25})_{2/3}(Ca_{0.8}Sr_{0.2})_{1/3}MnO_3$ compound (α and α′) are found to be 0.495 and 0.486 respectively, and these value agree well with that obtaining using tricritical mean-field [28].

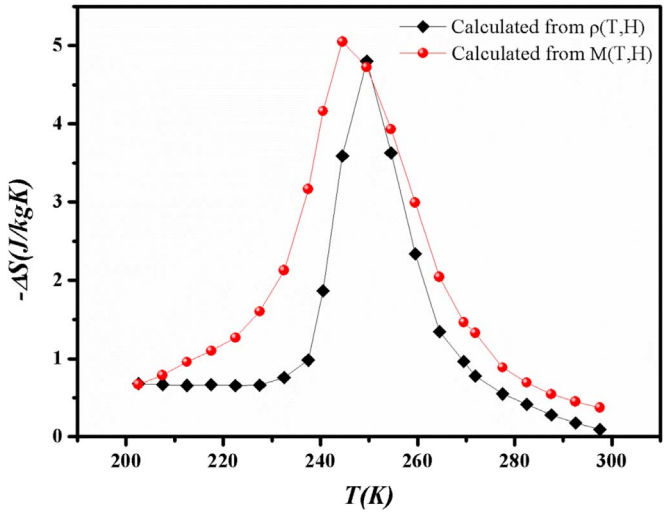

Fig. 4. Temperature dependence of the magnetic-entropy change ($-\Delta S_M$) measured and calculated for an applied magnetic field of 3 T for $(La_{0.75}Nd_{0.25})_{2/3}(Ca_{0.8}Sr_{0.2})_{1/3}MnO_3$ sample.

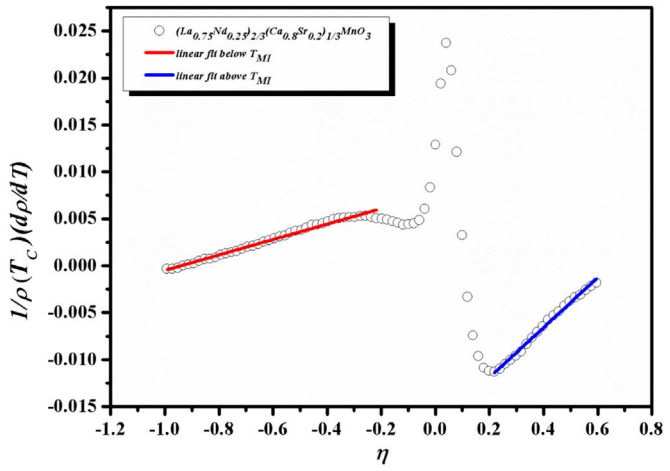

Fig. 5. The thermal derivative of resistivity normalized with respect to resistivity value at T_{Mi}, as a function of reduced temperature [$\eta=(T-T_{MI})/T_{MI}$].

Table 2
Values of different parameters used to fit the experimental data to Eqs. (4) and (5).

Sample	Region	A	B	α	β	γ
$(La_{0.75}Nd_{0.25})_{2/3}(Ca_{0.8}Sr_{0.2})_{1/3}MnO_3$	$T < T_{MI}$	0.00773	0.00822	α=0.495	0.215	–
	$T > T_{MI}$	−0.01723	0.02663	α′=0.486	–	1.124

3.3.2. Calculation of β and γ

Further, other critical exponents β and γ are calculated from the Suezaki-Mori model [29] which relates the temperature derivative of the electrical resistivity to the reduced temperature magnetic ordering (η) as follows:

$$\left[\frac{d\rho}{dT}\right] = -B_{+}\eta^{-(\alpha+\gamma-1)} \text{ for } T > T_{MI} \quad (7)$$

$$\left[\frac{d\rho}{dT}\right] = -B_{g}\eta^{-(\alpha+\gamma)/2} + B_{-}\eta^{-(\alpha+\gamma-1)} \text{ for } T < T_{MI} \quad (8)$$

Where the constants $B+$, $B-$ incorporate term involving the zone boundary energy gap B_g and η is the reduced temperature $[(T-T_{MI})/T_{MI}]$, as already denoted. Taking natural logarithm on both the sides, the Eq. (8) can be rewritten as:

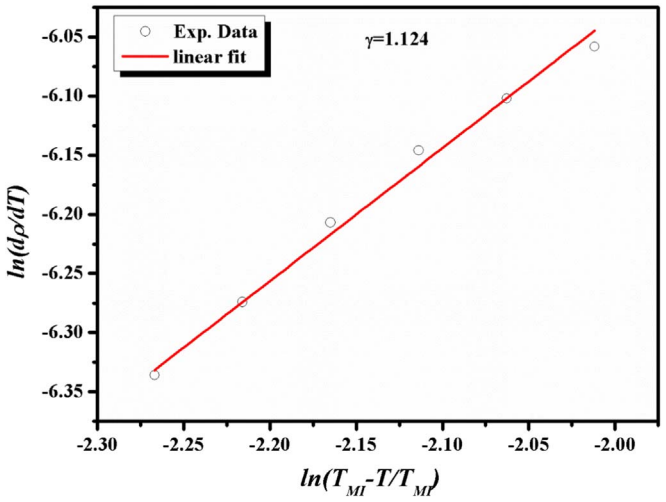

Fig. 6. ln(dρ/dT) vs ln $[(T-T_{MI})/T_{MI}]$ below T_{MI} under 3 T applied field.

$$Ln\frac{d\rho}{dT} = (\alpha+\gamma-1)Ln(\eta) \text{ for } T > T_{MI} \quad (9)$$

The slope of ln(dρ/dT) versus ln(η) plot gives the value of (α+γ−1). As α is obtained from the fit to the Fisher–Langer method, we can obtain the value of γ.

Fig. 6 shows ln(dρ/dT) vs ln(η) above T_{MI} and gives the value of (α+γ−1). The critical exponent obtained is γ=1.124 for $(La_{0.75}Nd_{0.25})_{2/3}(Ca_{0.8}Sr_{0.2})_{1/3}MnO_3$ sample.

The first term in Eq. (8) involving B_g will be dominant at temperatures less than T_{MI} because the scaling law gives (α+γ)/2−(α+γ−1)=β. As done earlier, the Eq. (8) can be also rewritten by taking natural logarithm on both sides.

$$Ln\frac{d\rho}{dT} = \left[\left(\frac{\alpha+\gamma}{2}\right) - (\alpha+\gamma-1)\right]Ln(\eta) \text{ for } T < T_{MI} \quad (10)$$

The direct slope of ln(dρ/dT) versus ln(η) below T_{MI} gives β=0.215 for $(La_{0.75}Nd_{0.25})_{2/3}(Ca_{0.8}Sr_{0.2})_{1/3}MnO_3$ sample as depicted in Fig. 7. The much deviation in the experimental points from the linear fit curves is due to the plotting in very narrow reduced temperature range below T_{MI} and also, of course, because the sample is polycrystalline.

Finally, one can see that Rushbrooke scaling relation α+2β+γ=2 [30] for $(La_{0.75}Nd_{0.25})_{2/3}(Ca_{0.8}Sr_{0.2})_{1/3}MnO_3$ sample is also satisfied and the value obtained is 2.049.

The exponents values obtained from the resistivity measurements for $(La_{0.75}Nd_{0.25})_{2/3}(Ca_{0.8}Sr_{0.2})_{1/3}MnO_3$ are very close to the ones

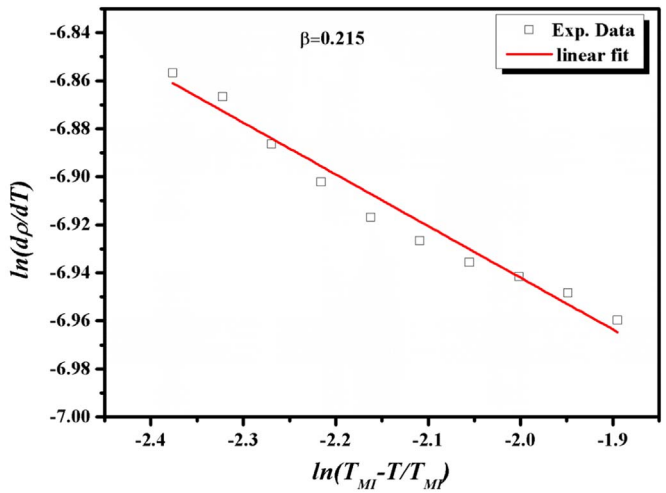

Fig. 7. ln(dρ/dT) vs ln $[(T-T_{MI})/T_{MI}]$ above T_{MI} under 3 T applied field.

predicted from the tricritical mean-field model. These results are similar to the analysis of critical exponents from the magnetization measurements [31].

4. Conclusion

In conclusion, the relation between magnetic entropy change and resistivity has been studied. It is noted that there is a strong correlation between ΔS_M extracted from magnetic and electrical measurements in $(La_{0.75}Nd_{0.25})_{2/3}(Ca_{0.8}Sr_{0.2})_{1/3}MnO_3$ manganite in the vicinity of the phase transition temperature. The little difference between these two methods can be explained not only by the strong electron–phonon interactions, but also by the effect of disorder. Also, we have examined the critical behavior from resistivity for $(La_{0.75}Nd_{0.25})_{2/3}(Ca_{0.8}Sr_{0.2})_{1/3}MnO_3$ sample under 3 T magnetic field. The estimation of critical exponents suggests the long range ferromagnetic order by having the tricritical mean-field model in agreement with the analysis of critical exponents from magnetization measurements.

Acknowledgments

This work is performed with in the frame work of collaboration and is supported by the Tunisian Ministry of Higher Education and Scientific Research and Technology and Higher Education, Scientific of French.

References

[1] M. Triki, E. Dhahri, E.K. Hlil, Mater. Lett. 84 (2012) 48–51.
[2] Y. tokura (Ed.)Colossal-magnetoresistive Oxides, Gordon & Breatch Science Publishers, 1999.
[3] F. Elleuch, M. Triki, M. Bekri, E. Dhahri, E.K. Hlil, J. Alloy. Compd. 620 (2015) 249–255.
[4] C.M. Xiong, J.R. Sun, Y.F. Chen, B.G. Shen, J. Du, Y.X. Li, J. IEEE Trans. Magn. 41 (2005) 122.
[5] Mounira Abassi, N. Dhahri, J. Dhahri, E.K. Hlil, Chem. Phys. 436–437 (2014) 40–45.
[6] Dhahbi Tlili, Sobhi Hcini, Michel Boudard, Sadok Zemni, J. Alloy. Compd. 657 (2016) 601.
[7] Abd El-Moez A. Mohamed, B. Hernando, A.M. Ahmed, Solid State Commun. 233 (2016) 15.
[8] J.C. Debnath, A.M. Strydom, P. Shamba, J.L. Wang, S.X. Dou, J. Appl. Phys. 113 (2013) 233903.
[9] S. Ghodhbane, E. Tka, J. Dhahri, E.K. Hlil, J. Alloy. Compd. 600 (2014) 172.
[10] M. Nasri, M. Triki, E. Dhahri, E.K. Hlil, P. Lachkar, J. Alloy. Compd. 576 (2013) 404–408.
[11] Ma Oumezzine, S. Zemni, O. Peña, J. Alloy. Compd. 508 (2010) 292.
[12] J.C. Debnath, R. Zeng, J.H. Kim, S.X. Dou, J. Alloy. Compd. 509 (2011) 3699.
[13] J.C. Debnath, R. Zeng, A.M. Strydom, J.Q. Wang, S.X. Dou, J. Alloy. Compd. 555 (2013) 33.
[14] J. Khelifi, A. Tozri, E. Dhahri, E.K. Hlil, J. Supercond. Nov. Magn. 26 (2013) 3133.
[15] A. Arulraj, P.N. Santhosh, R.S. Gopalan, J. Phys.:Condens. Matter 10 (1998) 8497.
[16] H.M. Rietveld, J. Appl. Cryst. 2 (1965) 65.
[17] A. Guinier, X. Dunod (Ed.)Théorie et Technique de la radiocristallographie3rd ed. (1964), 1964, p. 462.
[18] S. Das, T.K. Dey, J. Phys. D: Appl. Phys. 40 (2007) 185.
[19] J. O'Donnell, M. Onellion, M.S. Rzchowski, J.N. Eckstein, I. Bozovic, J. Phys. Rev. B 54 (1996) 6841.
[20] B. Chen, C. Uher, D.T. Orelli, J.V. Mantese, A.M. Mance, A.L. Micheli, J. Phys. Rev. B 53 (1995) 5094.
[21] M. Patra, K. De, S. Majumdar, S. Giri, J. Appl. Phys. Lett. 94 (2009) 092506.
[22] J. Khelifi, A. Tozri, E. Dhahri, Appl. Phys. A 1051 (2014) 116.
[23] J. Khelifi, A. Tozri, F. Issaoui, E. Dhahri, E.K. Hlil, Ceram. Int. 40 (2014) 1641.
[24] R. Skini, M. Khlifi, M. Triki, E. Dhahri, E.K. Hlil, Chem. Phys. 452 (2015) 67.
[25] K. Huang, Statistical Machanics, 2nd ed., Wiley, New York, 1987.
[26] S.N. Kaul, J. Magn. Magn. Mater. 53 (1985) 5.
[27] J.M.E. Fisher, J.S. Langer, Phys. Rev. Lett. 20 (1968) 665.
[28] (a) J.C. LeGuillou, J. Zinn-Justin, Phys. Rev. B 21 (1980) 3976;
(b) S.G. Gorishny, S.A. Larin, F.V. Tkachov, Phys. Lett. 101A (1984) 120.
[29] Y. Suezaki, Y. Mori, Prog. Theor. Phys. 41 (1969) 1177.
[30] (a) M.H. Coopersmith, Phys. Rev 167 (1968), 1968, p. 478;
(b) H. Eugene Stanley, Introduction to Phase Transitions and Critical Phenomena, Oxford University Press, New York, 1971;
(c) Igor Herbut, A Modern Approach to Critical Phenomena, Cambridge University Press Science, 2007.
[31] J. Khelifi, A. Tozri, F. Issaoui, E. Dhahri, E.K. Hlil, J. Alloy. Compd. 584 (2014) 617.